LITHOSPHERIC MODELLING BY USING

OPTIMIZED GOCE GRAVITY GRADIENT DATA

Benjamin D. Gutknecht

Christian-Albrechts-Universität zu Kiel, Institute of Geosciences, Otto-Hahn-Platz 1, DE-24118 Kiel, Germany, Email: benjamin@geophysik.uni-kiel.de

ABSTRACT

The observed gravity and gravity gradient tensor components from the GOCE mission add new dimension to the interpretation of lithospheric and mantle structure. Here we present two applications of GOCE data to solid Earth modelling: For the M_W=8.9 11th March 2011 earthquake offshore Sendai, Japan, GOCE gravity data has been used as a regional field in order to identify positive residual gravity anomalies close to the earthquake epicentre. Such anomalies are suspected of having significant influence on the stress regime of the subduction-zone interface. Concerning density modelling, it is of much interest to investigate density contrast and spatial distribution of the smallest density anomalies detectable with the GOCE gradiometer system. Allowing for accuracies of a few mE (1 milli-Eötvös = 10e-12 1/s²) and 1-1000 mGal (1 mGal = 10e-5 m/s²), we derived a relation for the diameter of a density anomaly located below the Geoid as a function of density contrast. However, this method does *not* consider spatial resolution of the sampled GOCE data but rather takes the sensitivity of the system into account. Thus, our results indicate what minimum size and density contrast of the underlying geophysical structures are required in order to produce a signal of the order of GOCE's gradiometer sensitivity. These findings can have considerable impact on forward modelling and interpretation due to the fact that they suggest lower boundary conditions for the size of geophysical structures to be modelled. Consequent 3D density modelling tests with a synthetic model of the Chilean-Pacific convergent margin show that gravity gradients and invariants upward continued to orbit height clearly outperform the gravity field in terms of information yield on location and shape of anomalous structures.

1. MOTIVATION

In the literature, large subduction-zone earthquakes have repeatedly been linked to diverse geological scenarios as subducted seamounts [1] or strong crust in the overriding plate [2], [3]. Following the idea described in [3] that positive density anomalies in the overlaying continental crust of subduction zones can have significant impact on the locking of a subduction zone interface, we investigated whether the GOCE satellite has sufficient instrument sensibility in order to provide gravity (and gravity gradient) data that can be used for crustal studies related to major earthquakes.
It is assumed that positive density anomalies in the forearc region of the erosive subduction zone of the central Andes can be related to Jurassic-Early Cretaceous batholithic structures [4], [5]. Since these anomalies can be shown to be located near the epicentres of large earthquakes [3], [section 2.1], it is of much interest to assess potential use of GOCE-derived gravity data for identification of suchlike structures.

2. METHODS AND RESULTS

Here we use two different approaches to make use of GOCE gravity field data. In section 2.1 GOCE gravity data is being used as regional gravity field in order to calculate a residual Bouguer gravity anomaly field for the M_W=8.9 earthquake of 11th March 2011 offshore Sendai, Japan. In section 2.2 it is evaluated what size and density contrast a batholithic structure must have in order to generate an anomaly signal in the order of the satellite's accuracy.

2.1. Gravity residuals offshore Sendai

For the M_W=8.9 Sendai earthquake the EGM 2008 gravity field [6] and the GOCE GCF2 direct approach gravity field (release 2 of March 2011 via http://icgem.gfz-potsdam.de/ICGEM) were used in order to calculate residual fields for the region between 135-150°E and 30-45°N. The residual field was calculated by subtracting the simple Bouguer anomaly field of the GOCE data from the simple Bouguer anomaly field of the EGM2008 data. The expected result for the residual field is a high-pass filter like effect so that only short wave content remains. The GOCE data thereby acts as a regional gravity field which primarily comprises the gravity effects of longer wavelength structures greater than 80 km, i.e. of subduction slabs, mountain ranges etc.
Fig. 1 gives an overview of the Japan-Pacific collision zone centred at the epicentre as given by [7]. Fig. 2 shows the residual Bouguer anomaly field after the GOCE-derived field has been subtracted from the EGM 2008 field.

Proc. of '4th International GOCE User Workshop', Munich, Germany 31 March – 1 April 2011 (ESA SP-696, July 2011)

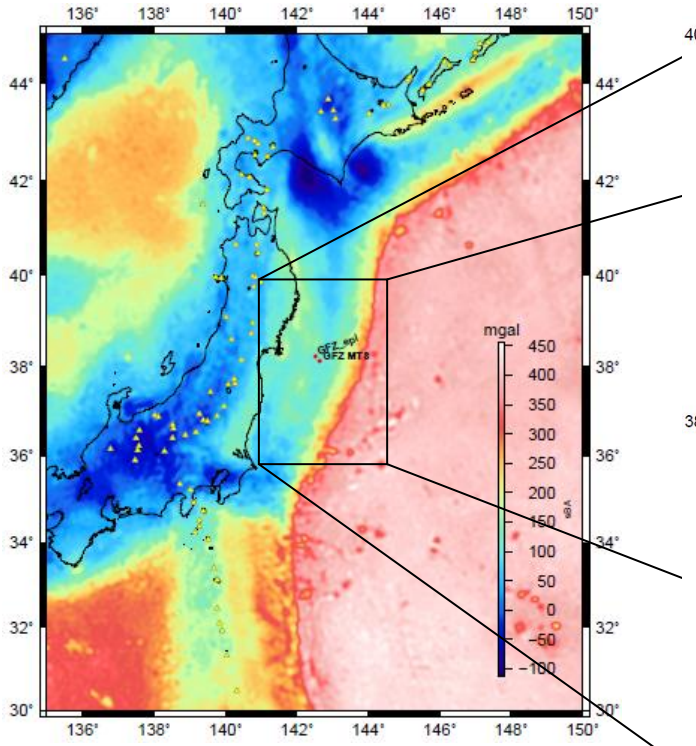

Figure 1. Bouguer gravity anomaly map of the Japan-Pacific continental margin (EGM 2008). Yellow triangles denote volcanoes. GFZ locations for epicentre (GFZ_epi) and moment tensor solution (GFZ_MTS) of the 11th March 2011 Sendai earthquake are given as red dots, respectively. The black square defines the location of Fig. 2. 1 mgal = 10^{-5}m s^{-2}.

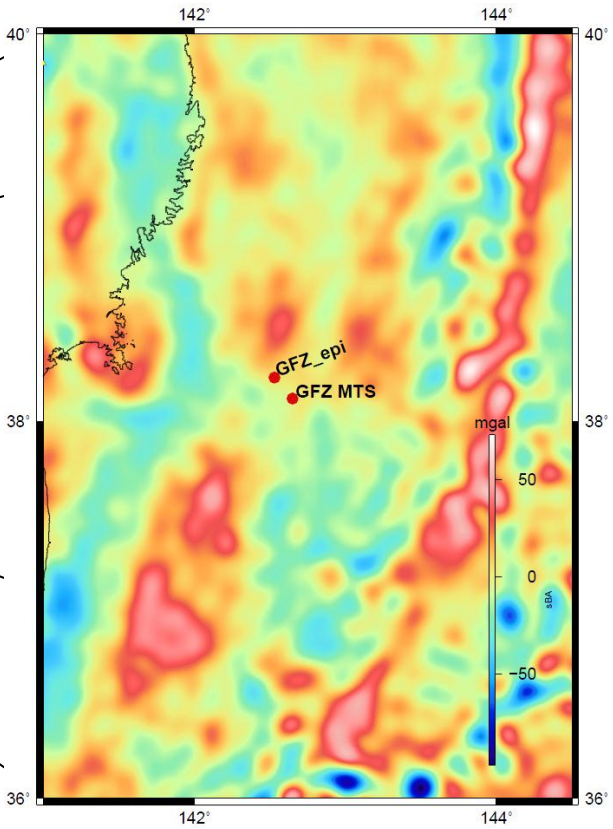

Figure 2. Residual Bouguer anomaly map of the Japan-Pacific continental margin after the GOCE gravity field has been subtracted from EGM 2008. GFZ locations for epicentre (GFZ_epi) and moment tensor solution (GFZ_MTS) of the 11th March 2011 Sendai earthquake are given as red dots, respectively.

The epicentre is clearly situated at the edge of a positive residual Bouguer anomaly.

2.2. Sensitivity analysis with a simple spherical density residual

In order to derive an equation that gives us the minimum parameter configuration, i.e. density contrast and size of a gravity anomaly so that it generates at least a signal in the order of the sensitivity of the satellite gradiometer (or gravity field), we start with the most simple geometry: a spherical density anomaly located directly below the geoid (Fig. 3).

2.2.1. d/Δρ-ratio for fixed gravity accuracy

Starting from Newtonian gravity acceleration

$$g_{Newton} = G \cdot m \cdot R^{-2} = G \cdot V \cdot \Delta\rho \cdot R^{-2}, \quad (1)$$

with *gravitational constant* $G=6.67\times10^{-11}Nm^2kg^{-2}$, *mass* m, *distance* $R=254.9\times10^3m$, *volume* V and *density contrast* $\Delta\rho=\rho_1-\Delta\rho_2$,

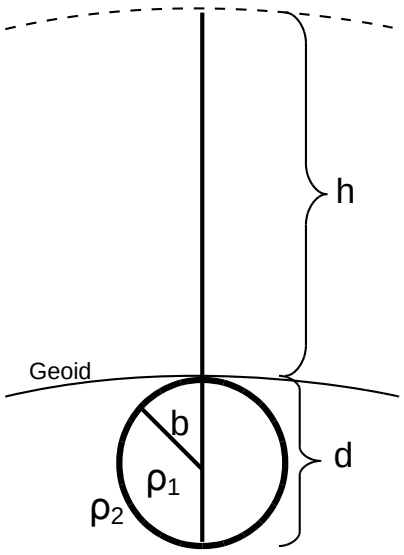

Figure 3. Simple spherical model of a batholithic density residual structure with diameter d=2b and density contrast $\Delta\rho=\rho_1-\rho_2$, located directly below the geoid. The satellite orbit height above the geoid is assumed as being constant with h=254.9 km.

the vertical residual anomaly of a sphere with diameter

$$d = 2b \tag{2}$$

in the order of the instrument sensitivity Δg_z is defined as

$$\begin{aligned}\Delta g_z &= G \cdot \frac{4}{3}\pi b^3 \Delta\rho \cdot z^{-2} \\ &= \frac{4}{3}\pi G \cdot \Delta\rho \cdot \frac{b^3}{(h+b)^2}\end{aligned} \tag{3}$$

that eventually becomes Eq. 4 which gives us the minimum density contrast with respect to the anomaly radius (Eq. 4a) and diameter (Eq. 4b), respectively:

$$\overset{\Delta g_z = const.}{\Leftrightarrow} \quad \Delta\rho(b) = \frac{3}{4}\frac{\Delta g_z}{\pi G} \cdot \frac{(h+b)^2}{b^3} \tag{4a}$$

$$\overset{\Delta g_z = const.}{\Leftrightarrow} \quad \Delta\rho(d) = \frac{3}{4}\frac{\Delta g_z}{\pi G} \cdot \frac{\left(h+\frac{d}{2}\right)^2}{\frac{d}{2}^3} \tag{4b}$$

2.2.2. d/Δρ-ratio for fixed vertical gradient accuracy

For the vertical gravity gradient, we do basically the same, again starting from Newton

$$\frac{\partial g_{Newton}}{\partial R} = -2 \cdot G \cdot m \cdot R^{-3} \tag{5}$$

and at right angle on top of the spherical residual anomaly in Cartesian coordinates

$$\begin{aligned}\Delta g_{zz} &= \frac{\partial}{\partial z}\left(G \cdot V \cdot \Delta\rho \cdot z^{-2}\right) \\ &= -2 \cdot G \cdot V \cdot \Delta\rho \cdot z^{-3} \\ &= -2 \cdot G \cdot \frac{\frac{4}{3}\pi b^3 \Delta\rho}{(h+b)^3} \\ &= -\frac{8}{3}\pi \cdot G \cdot \Delta\rho \cdot \frac{b^3}{(h+b)^3}\end{aligned} \tag{6}$$

And just as for the gravity case, we assume a fixed sensitivity. On the long run, a value of 12 mE (*1 mili-Eötvös=$10^{-9}s^{-2}$)* seems achievable within the measurement bandwidth [8].

Equation 7a and 7b then respectively give the relation for the minimum density contrast with respect to the anomaly radius and diameter in order to produce a residual signal in the order of Δg_{zz}.

$$\overset{\Delta g_{zz} = const.}{\Leftrightarrow} \quad \left|\Delta\rho(b)\right| = \frac{3}{8}\frac{\Delta g_{zz}}{\pi G} \cdot \frac{(h+b)^3}{b^3} \tag{7a}$$

$$\overset{\Delta g_{zz} = const.}{\Leftrightarrow} \quad \left|\Delta\rho(d)\right| = \frac{3}{8}\frac{\Delta g_{zz}}{\pi G} \cdot \frac{\left(h+\frac{d}{2}\right)^3}{\left(\frac{d}{2}\right)^3} \tag{7b}$$

Equations 4b and 7b allow an evaluation of the gravity and gravity gradient sensibility, respectively. Fig. 4 compares different residual values of 1 and 10 mgal (1 mgal = 10^{-5}m s^{-2}), and 12, 24 36 and 1000 mE, respectively. Assuming target values of 1 mgal for the gravity field and 12 mE for the vertical gravity gradients, it can be found that the gradients clearly outperform the gravity field. For a given density contrast, the gravity field 'needs' a structure about twice the size as for the gradient case. Depending on density contrast in the order of 30 to 200 kg m^{-3}, the smallest resolvable anomaly in the gradient domain (with respect to accuracy, not space) is then some 30 to 45×10^3 m. Yet a level of 24 or 36 mE in this study gives better results for the gradients than for 1 mgal gravity.

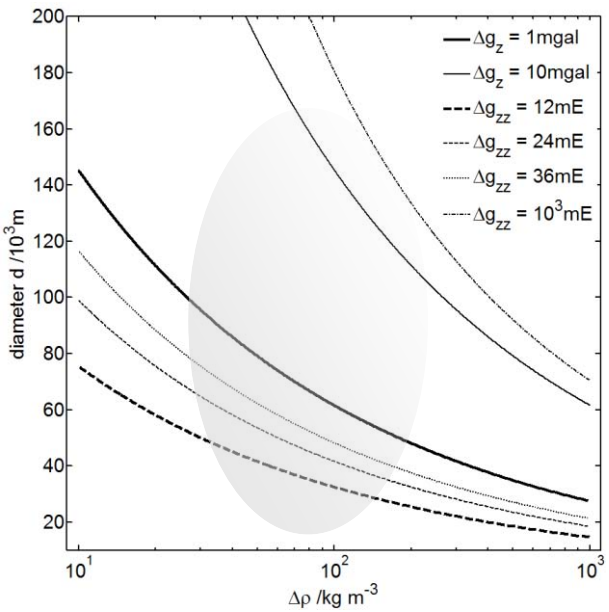

Figure 4. Density contrast versus minimum diameter of a density anomaly generating a residual anomaly in the order of given instrument /field accuracies. Areas below and to the left of the curves cannot be resolved. Gradients of GOCE outperform gravity. The grey shaded area depicts appropriate parameter ranges of possible batholithic structures. In practice, signals 2-3 times the sensitivity amplitude will be required in order to be distinguished from the background level.

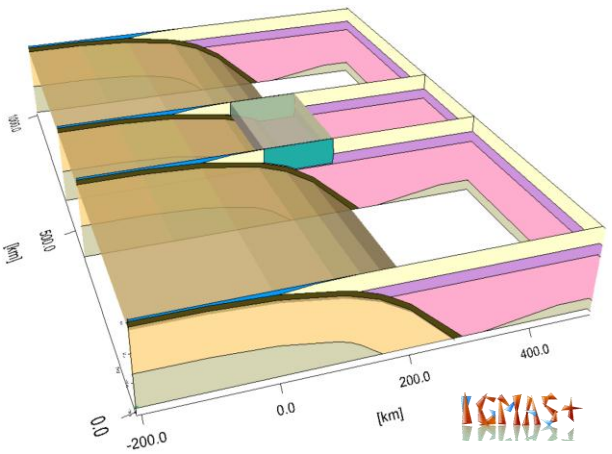

Figure 5. Synthetic 3D density model of a Chilean-type subduction zone ('shoe-box model'). There is no varying topology along the strike of the subduction zone. The green coloured 'shoe box' inset in the centre is a simple analogy to a continental crust positive density anomaly simulating a batholithic structure.

2.2.3. SYNTHETIC 3D FORWARD MODELLING

Subsequently to the rather abstract computations of sections 2.2.1 and 2.2.2, 3D density forward modelling of gravity and full tensor gravity gradients has been applied in order to estimate the anomaly signal strength at both near surface and orbit height. The density model (Fig. 5) is based on existing models of the Chilean-Pacific margin by [9]. Unlike 'real' models, the geometry used for this study does not show any variability along the N-S-axis and rather synthesises arbitrary constant average-subduction zone geometry along strike. Within this geometry lies a 'shoe-box' like dummy structure to simulate a giant batholithic density anomaly. The dimensions of the structure are considerably oversized (125km × 200km × 30km, density contrast ~100-300 kg m^{-3}) and somewhat depicting an upper feasible boundary in a geological sense of size. The inset body's dimension was deliberately chosen large so that negative modelling results would implicitly lead to no further testing when even the largest feasible density anomaly generated no notable signal when measured at orbit height.

Model construction and forward modelling was performed using the modelling software IGMAS+, which represents geological bodies with triangular-faceted polyhedral [10], [11].

The calculated vertical gravity Bouguer anomaly is shown in Fig. 6 (left) at near surface and in Fig. 6 (right) at orbit height ($h=254.9\times10^3 m$). The gravity signal of the density anomaly is apparently orders of magnitude too weak to be seen from orbit (cf. Fig. 6 right).

The vertical gravity gradient g_{zz}, however, clearly yields amplitudes from the 'shoe-box' in the detectable range (cf. Fig. 7).

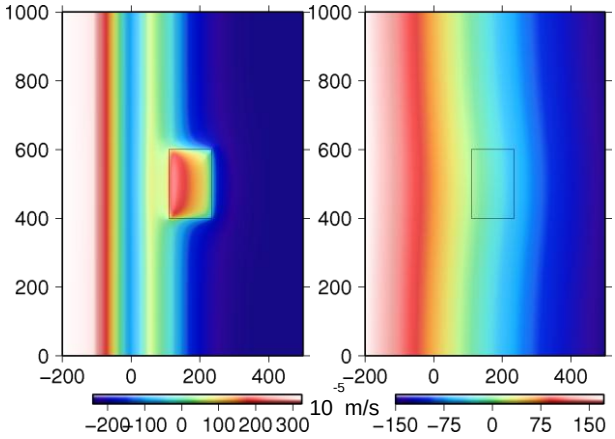

Figure 6. Bouguer anomaly of the vertical gravity component (g_z) above the Andean-type density model of Fig. 5; near surface (l) and at GOCE orbit height (254.9 km, r). Map scale is in km. The amplitude range of the orbit-gravity field is more than 12 times higher than the anomaly maximum of the 'shoe-box'.

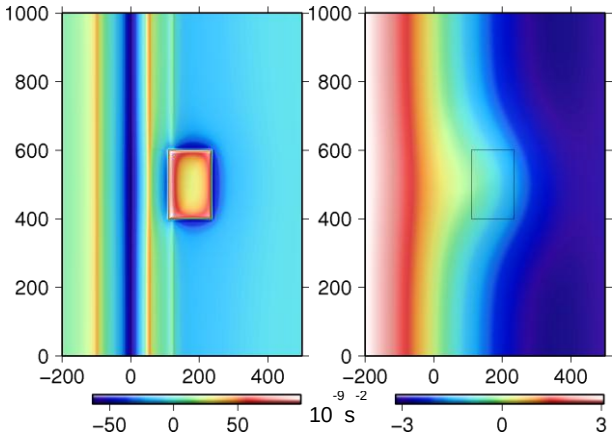

Figure 7. The vertical gravity gradient (g_{zz}) of the same model near surface (l) and at orbit (r). Map scale in km. The amplitude range of the orbit-gradient field is only 3.5 times higher than the anomaly signal.

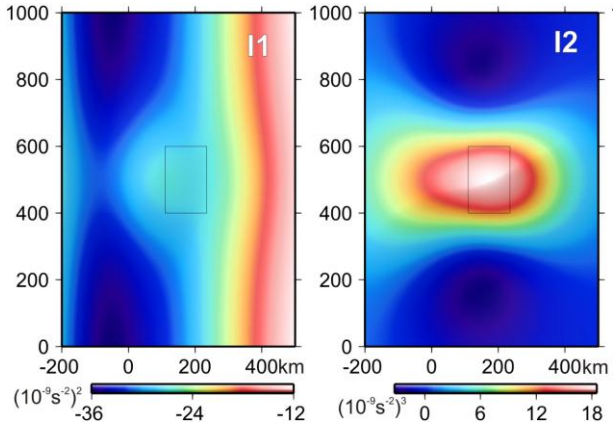

Figure 8. Invariants of the full gravity gradient tensor at orbit height. I2, i.e. the determinant of the tensor, reveals to be a promising tool for anomaly localisation.

3. DISCUSSION & SUMMERY

Both GOCE gravity and gravity gradient data can be shown to have notable potential for respective, characteristic use. While gravity unsurprisingly fails to be directly usable for the detection of batholithic structures in the overriding crust of subduction zones it has great potential to be applied as regional field during the computation of gravity residual anomaly maps. This application can be recommended if the wavelength of suspected anomalies lies below 80-100 km. Regarding the Sendai earthquake of 11th March 2011, GOCE gravity data helped to identify positive gravity anomaly residuals at the epicentre of the main shock. A possible interpretation of these residuals as high density bodies in the upper plate, affecting the subduction interface, is supported by the existence of large positive anomalies found in aero-magnetic data [12].

However, the gravity gradients show high potential for their use within direct localisation purposes if their proposed noise levels will be matched. For a simple spherical model it was shown that gravity gradients – for given accuracies – are more sensitive to small scales and density contrasts than gravity even at GOCE's orbit. Subsequent 3D forward modelling results support these theoretic estimations: The simulated signal of a synthetic density anomaly at a subduction zone disappears in the amplitudes of the surrounding geology. But the signal can clearly be found in the calculated gravity gradients.

Furthermore, invariants of the full gradient tensor are a promising tool for anomaly localisation purposes. A combination of all tensor elements leads to a somewhat easier-to-read picture when compared to gradients, is independent of the coordinate system but lacks direct physical interpretability.

Altogether, the findings of this study encourage to call for an originally unintended release of GOCE gradient grid data by ESA. Nevertheless, for the purposes presented in this paper, GOCE gravity field data is by all means suitable for earthquake studies when it is used as a regional field.

4. ACKNOWLEDGEMENT

Many thanks to Roland Pail at IAPG/Technische Universität München, who provided information on the accuracy of GOCE gradients. As well many thanks to Monika Sobiesiak, Rezene Mahatsente and H.-J. Götze at the Institute of Geosciences/Christian-Albrechts-Universität zu Kiel, for in-depth discussion on subduction-zone seismicity, stress regime and rheology. Part of this work has been accomplished during the author's Ph.D. time and part of this work has been financed through project IMOSAGA within the German Research Foundation (DFG) priority programme SPP1257 Mass Transport and Mass Distribution.

5. REFERENCES

1. Cloos, M. (1992). Thrust-type subduction-zone earthquakes and seamount asperities: A physical model for seismic rupture. *Geology*, 20, 601-604.
2. Byrne, D.E. et al. (1988). Loci and maximum size of thrust earthquakes and the mechanics of shallow region of subduction zones. *Tectonics*, 7, 833-857.
3. Sobiesiak, M. et al. (2007). Asperity generating upper crustal sources revealed by b value and isostatic residual anomaly grids in the area of Antofagasta, Chile. *JGR*, 112, B12308.
4. Götze, H.-J. et al. (1994). The lithospheric structure of the central Andes (20-26° S) as inferred from interpretation of regional gravity, in *Tectonics of the Southern Central Andes, Structure, and Evolution of an Active Continental Margin*, edited by K.J. Reutter, E. Scheuber, and P.J. Wigger, pp. 7-22, Springer Verlag, New York.
5. Götze, H.-J. & Krause, S. (2002). The central Andean gravity high, a relic of an old subduction complex?, *J. S. Am. Earth Sci.*, 14, 799.
6. Pavlis, N.K. et al. (2008). *An Earth Gravitational Model to Degree 2160: EGM2008*. EGU General Assembly 2008
7. GFZ Potsdam / GEOFON / Global Seismic Monitor at *http://geofon.gfz-potsdam.de/geofon//*
8. Pail, R., *pers.comm.*
9. Tašárová, Z. (2007). Towards understanding the lithospheric structure of the southern Chilean subduction zone (36°S-42°S) and its role in the gravity field. *Geophys. J. Int.*, 170, 3, 995 1014.
10. Götze, H.-J. & Lahmeyer, B. (1988). Application of three-dimensional interactive modeling in gravity and magnetics. *Geophysics*, 53(8): 1096-1108.
11. Schmidt, S. et al. (submitted). Hybrid modelling of gravity, gravity gradients and magnetic fields., submitted for the *Geophys. Prosp. EGM 2010 CAPRI Special Issue "Advances in Electromagnetic, Gravity and Magnetic Methods for Exploration".*
12. Finn, C. (1994). Aeromagnetic evidence for a buried Early Cretaceous magmatic arc, northeast Japan. *JGR*, 99, B11, 165-185.